Contrib Mineral Petrol (2011) 161:597–613
DOI 10.1007/s00410-010-0552-9

ORIGINAL PAPER

The mobility of U and Th in subduction zone fluids: an indicator of oxygen fugacity and fluid salinity

Enikő Bali · Andreas Audétat · Hans Keppler

Received: 21 June 2010 / Accepted: 29 June 2010 / Published online: 15 July 2010

Abstract The solubility of U and Th in aqueous solutions at P-T-conditions relevant for subduction zones was studied by trapping uraninite or thorite saturated fluids as synthetic fluid inclusions in quartz and analyzing their composition by Laser Ablation-ICPMS. Uranium is virtually insoluble in aqueous fluids at Fe-FeO buffer conditions, whereas its solubility increases both with oxygen fugacity and with salinity to 960 ppm at 26.1 kbar, Re-ReO_2 buffer conditions and 14.1 wt% NaCl in the fluid. At 26.1 kbar and 800°C, uranium solubility can be reproduced by the equation: $\log U = 2.681 + 0.1433 \log fO_2 + 0.594Cl$, where fO_2 is the oxygen fugacity, and Cl is the chlorine content of the fluid in molality. In contrast, Th solubility is generally low (<10 ppm) and independent of oxygen fugacity or fluid salinity. The solubility of U and Th in clinopyroxene in equilibrium with uraninite and thorite was found to be in the order of 10 ppm. Calculated fluid/cpx partition coefficients of Th are close to unity for all conditions. In contrast, $D^{fluid/cpx}$ for uranium increases strongly both with oxygen fugacity and with salinity. We show that reducing or NaCl-free fluids cannot produce primitive arc magmas with U/Th ratio higher than MORB. However, the dissolution of several wt% of oxidized, saline fluids in arc melts can produce U/Th ratios several times higher than in MORB. We suggest that observed U/Th ratios in arc magmas provide tight constraints on both the salinity and the oxidation state of subduction zone fluids.

Keywords Synthetic fluid inclusions · Subduction · U-Th decoupling · Oxygen fugacity · LA-ICPMS · Arc magmas

Communicated by J. Hoefs.

Electronic supplementary material The online version of this article (doi:10.1007/s00410-010-0552-9) contains supplementary material, which is available to authorized users.

E. Bali (✉) · A. Audétat · H. Keppler
Bayerisches Geoinstitut, University of Bayreuth, Universitätstrasse, 30, 59447 Bayretuh, Germany
e-mail: eniko.bali@uni-bayreuth.de

A. Audétat
e-mail: andreas.audetat@uni-bayreuth.de

H. Keppler
e-mail: hans.keppler@uni-bayreuth.de

Introduction

The behavior of U and Th has been of great interest in many fields of Earth sciences such as economic geology, geochronology, environmental science and igneous geochemistry. In the latter, one interesting aspect is the variable degree of enrichment of U vs. Th in silicate melts of different tectonic settings. It has long been noted that primitive volcanic arc lavas typically have higher U/Th ratios than lavas in rift settings and hypothetic partial melts of spinel or garnet peridotite (e.g., Pearce and Peate 1995; Hakesworth et al. 1997, for a review). We confirmed this general trend by an extensive compilation of primitive magma compositions reported from 26 subduction-related and 8 rift-related settings. Typical examples of an island arc, a continental arc and an intracontinental rift setting, are shown in Figs. 1a–c and are compared with the predicted compositions of partial melts of spinel and garnet lherzolite in Figs. 1d–e. Corresponding histograms for 25 other subduction-related and 7 other rift-related settings are shown in electronic Appendices 1 and 2.

The mobility of U in aqueous solutions at ambient (Langmuir 1976) and hydrothermal conditions (e.g.,

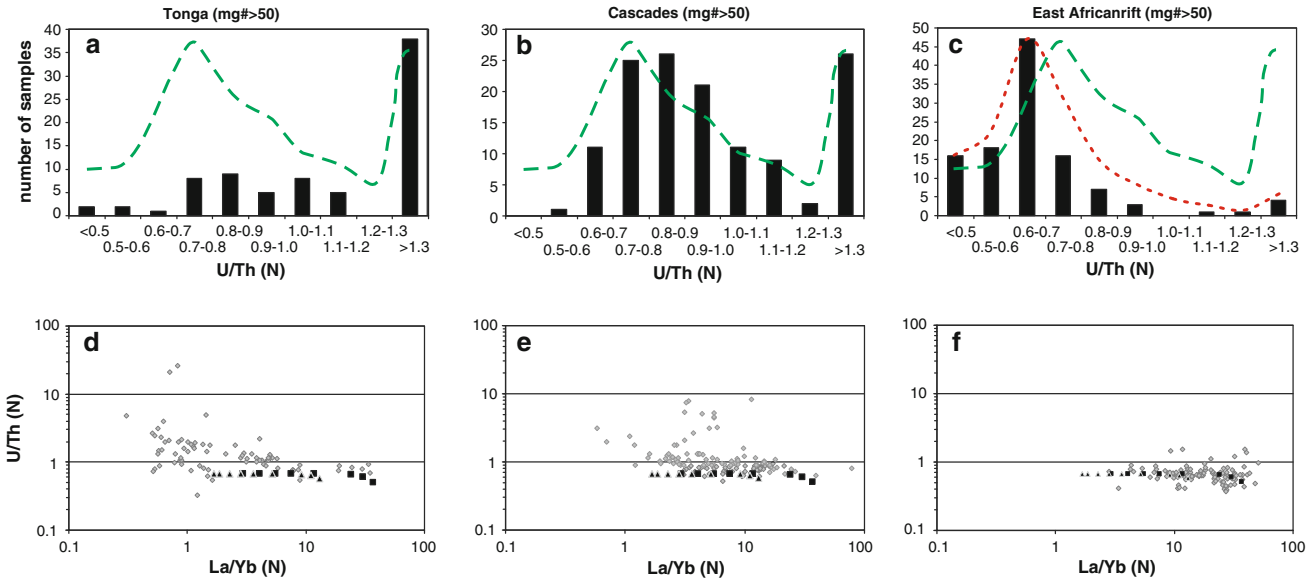

Fig. 1 Distribution of MORB-normalized (Hart et al. 1999) U/Th ratios in primitive basalts from three different tectonic environments: **a** Tonga, representative for a volcanic arc setting **b** Cascades, representative for a continental arc setting and **c** East African Rift, representative for a rift setting. Data source is the Georock database at http://georoc.mpch-mainz.gwdg.de/georoc/. The data were filtered to avoid strongly altered and fractionated rocks, using the following filtering conditions: mg# (calculated as $100 \times MgO/(MgO + FeO) > 50$, $LOI < 2$. Note the large proportion of samples with a U/Th(N) ratio >1.3 in the two subduction-related examples as opposed to the mostly low U/Th ratios in the samples from the East African Rift. *Dashed* and *dotted lines* indicate the general distribution of U/Th(N) ratios of volcanic arcs and rift volcanites based on 1,740 and 358 analyses, respectively. **d–f** La/Yb(N) versus U/Th(N) diagram of the same databases that were used for (**a–c**). La/Yb ratios are sensitive to the degree of partial melting and can thus be used to recognize a potential link between U/Th(N) and the degree of partial melting. Hypothetical partial melts of dry 4-phase spinel and garnet lherzolites (calculated based on the melting reactions of Walter 1998 and Kinzler and Grove 1992; partition coefficients of Salters et al. 2002; McKenzie and O'Nions 1991 and equations for non-modal fractional partial melting) show virtually no dependence of U/Th(N) on the degree of partial melting. Thus, the high and variable U/Th(N) values in the two arc-related examples are likely to reflect some subduction signature

Keppler and Wyllie 1991; Peiffert et al. 1994; Peiffert et al. 1996) depends strongly on oxygen fugacity, fluid pH and the availability of complex-forming anions. The mobility of Th, on the other hand, seems to be less affected by these variables, as suggested by fluid/melt partitioning experiments of Keppler and Wyllie (1990) and Keppler and Wyllie (1991). The differences between U and Th are due to differences in oxidation state. While both U and Th are poorly soluble in water in the +4 oxidation state, only U may be oxidized to U^{6+}, which is readily soluble in aqueous solutions as uranyl (UO_2^{2+}) cation. Based on the available experimental results and the observation that U behaves similarly to large ion lithophile elements (LILE; e.g., Ba, Rb, Cs Pb), it has been proposed that the enrichment of U over Th in volcanic arc lavas is inherited from the composition of subduction zone fluids (e.g., Stolper and Newman 1994; Hakesworth et al. 1997). Recently, it was suggested that instead of the effect of aqueous fluid, the presence of refractory allanite in the subducted slab might be responsible for this phenomena (Hermann 2002; Klimm et al. 2008; Hermann and Rubatto 2009).

The aim of this study is to determine the major factors controlling U and Th mobility in aqueous fluid at conditions relevant to subduction zones. We will then use these data to constrain both the salinity and the oxidation state of subduction zone fluids, two variables that are poorly constrained in current models. Toward this, we carried out U and Th solubility experiments in aqueous fluids at variable fO_2 conditions, fluid salinities and pressures at a constant temperature of 800°C. Small aliquots of fluid equilibrated with uraninite or thorite were trapped in form of synthetic fluid inclusions and subsequently analyzed by LA-ICPMS. Uraninite (UO_2) and thorite ($ThSiO_4$, isostructural to zircon) were found to be the stable phases of U and Th in equilibrium with both quartz and mantle minerals. To obtain realistic fluid compositions for mantle conditions, we also determined the solubility of U and Th in diopside and garnet in equilibrium with uraninite/thorite saturated fluid, which allow us to calculate the partition coefficients of U and Th between fluid and clinopyroxene and garnet. The advantage of this method is that in solubility experiments with pure uraninite and pure thorite, attainment of equilibrium is rapidly achieved by the complete dissolution

of an accessory phase, and it is not limited by the slow diffusion of U and Th in silicate minerals. This experimental approach does not imply that we assume the presence of accessory uraninite or thorite anywhere in the mantle or in the subducted slab. Rather, these minerals serve as convenient standard states for uranium and thorium activity.

Experimental procedure and analytical techniques

Starting materials and capsule preparation

Synthetic fluid inclusions were trapped in natural, inclusion-free quartz from Brazil. For each experiment, a quartz piece of ~7–30 mm^3 size was loaded into a $Pt_{95}Rh_{05}$ capsule together with a small grain of natural uraninite (UO_2) or thorite ($ThSiO_4$) and 23–40 µl H_2O (Fig. 2, Table 1). Our preliminary XRD studies suggested that UO_2 and $ThSiO_4$ are the stable phases in the experimental conditions, with $ThSiO_4$ having attained the structure of huttonite (monoclinic $ThSiO_4$). The aqueous fluid was spiked with 584–998 ppm Cs, Rb and Ba to provide internal standards for LA-ICPMS analysis, plus with 582–995 ppm Co to monitor the relative time sequence of fluid inclusion entrapment. The fluid salinity varied from 0 to 41.5 wt% NaCl. However, since Cs, Rb, Ba and Co were added in form of chlorides also the NaCl-free runs contain a small amount of Cl (0.14–0.25 wt%). Due to the addition of these minor components, the salinity is expressed as equivalent NaCl content ($NaCl_{equiv}$), in which the molar amount chlorine was recalculated as NaCl and added to the nominal NaCl contents. The $Pt_{95}Rh_{05}$ capsule design presented in Fig. 2a leads to minimal water loss during welding and during the experiments (Audetat and Bali 2010), which is essential for the internal standardization of the LA-ICPMS analyses. This is mostly due to the suppression of recrystallization of the platinum by rhodium. A few exploratory experiments were performed without fO_2 buffer, using $Pt_{95}Rh_{05}$ capsules of 5.0 mm outer diameter (O.D.), 4.4 mm inner diameter (I.D.) and 10.0 mm length (Fig. 2a, b). Subsequent fO_2-buffered experiments we performed using $Pt_{95}Rh_{05}$ capsules of 3.7 mm O.D., 3.2 mm I.D. and 8.0 mm length, which were placed in outer capsules made of Fe, Co or Ni (Fig. 2c). The space between the two capsules was filled with a slurry composed of the corresponding metal oxide and H_2O. For the Re-ReO_2 buffered elements, we used $Pt_{95}Rh_{05}$ for both the outer and the inner capsule and placed Re-foil, ReO_2 and H_2O in the space between (Fig. 2d). The outer capsules became closed during compression by cold welding.

For measuring the solubility of U and Th in diopside, approximately 40 mg of CMAS-oxide powder with aluminous diopside bulk composition (Table 2) was encapsulated with 11–17 ml of water and a uraninite or thorite grain in order to provide U or Th saturated fluid in equilibrium with the growing silicate minerals. The components of the powder were high purity oxides and Ca-carbonate. It was ground and mixed in an agate mortar under ethanol. The dry powder was slowly decarbonated in a high-temperature oven and kept at 1,000°C overnight. We used the same capsule design as for synthetic fluid inclusion experiments. The experiments were buffered by Co-CoO and Re-ReO_2, and fluid salinity was either 0 or 14.1 wt% NaCl (Table 2).

High-pressure experiments

The $Pt_{95}Rh_{05}$ capsules were kept in a drying oven overnight before the experiment and precisely weighted to check for possible water leaks. The experiments were carried out in an end-loaded piston cylinder apparatus

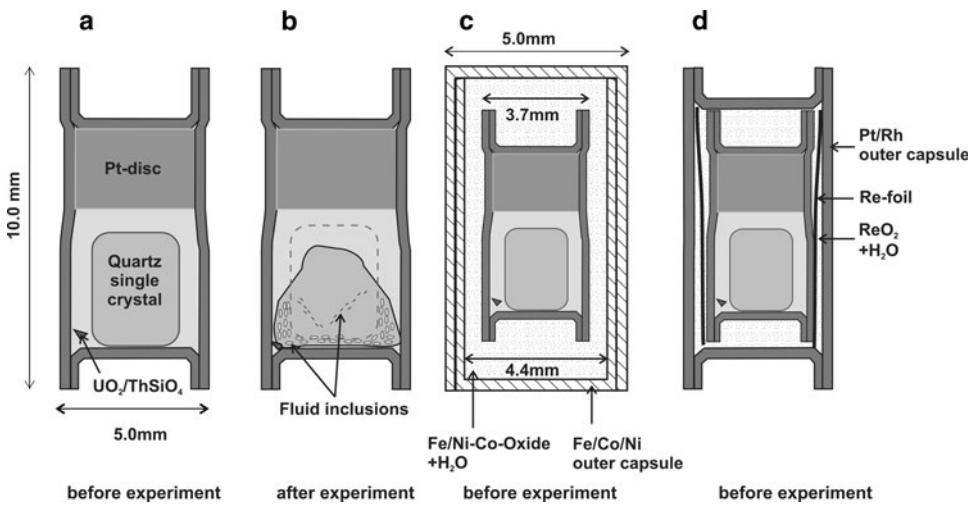

Fig. 2 Capsule designs for experiments without (**a**–**b**) and with (**c**–**d**) fO_2 buffer. The relatively thick Pt-disk in the inner capsule serves as mechanical seal during the welding of the top lid (Audetat and Bali 2010 for details). **b** Depicts the dissolution of original quartz in the center of the capsule and precipitation of new, fluid inclusion bearing quartz at the slightly cooler bottom of the capsule during the experiment

Table 1 Experimental details and results of synthetic fluid inclusion experiments

Sample nr	*P* (kbar)	Duration	Buffer	Capsule	Weight of starting material (g)			$NaCl_{eqiuv}$ in fluid (wt%)	Pressure cell	Nr of analyzed inclusions	Average concentration (ppm)	1 sigma st dev (%)
					Qz	UO_2	fluid					
#71	15	66 h	–	Pt/Rh, OD: 5.0 mm, L: 10.0 mm	0.07940	0.00135	0.03166	0.20	Pure NaCl	15	40	82
#72	15	94.5 h	–	Pt/Rh, OD: 5.0 mm, L: 10.0 mm	0.08068	0.00445	0.03113	1.50	Pure NaCl	14	20	107
#73	15	69 h	–	Pt/Rh, OD: 5.0 mm, L: 10.0 mm	0.08823	0.00373	0.03488	0.39	Pure NaCl	5	10	91
#74	15	69 h	–	Pt/Rh, OD: 5.0 mm, L: 10.0 mm	0.07606	0.01720	0.04095	14.10	Pure NaCl	9	550	54
#75	15	66.25 h	–	Pt/Rh, OD: 5.0 mm, L: 10.0 mm	0.13357	0.00329	0.02830	41.73	Pure NaCl	12	1350	27
#84	26.1	24 h	Re-ReO_2	Outer: Pt/Rh, inner: Pt/Rh	0.01689	0.00114	0.03050	14.10	MgO-NaCl	9	960	12
#85	26.1	24 h	Re-ReO_2	Outer: Pt/Rh, inner: Pt/Rh	0.02120	0.00106	0.02350	0.39	MgO-NaCl	12	20	30
#87	14.3	24 h	Re-ReO_2	Outer: Pt/Rh, inner: Pt/Rh	0.02134	0.00073	0.02828	14.10	MgO-NaCl	23	190	41
#89	7.1	24 h	Re-ReO_2	Outer: Pt/Rh, inner: Pt/Rh	0.02055	0.00069	0.02650	14.10	MgO-NaCl	7	110	21
#91	26.1	24 h	Fe-FeO	Outer: Fe, inner: Pt/Rh	0.02432	0.00061	0.02025	14.10	MgO-NaCl	8	<3	–
#92	26.1	24 h	Fe-FeO	Outer: Fe, inner: Pt/Rh	0.02068	0.00018	0.02270	0.39	MgO-NaCl	5	<2	–
#96	26.1	24 h	Co-CoO	Outer: Co, inner: Pt/Rh	0.02738	0.00189	0.01799	0.39	MgO-NaCl	5	7	38
#98b	26.1	24 h	Co-CoO	Outer: Co, inner: Pt/Rh	0.01821	0.00071	0.02495	14.10	MgO-NaCl	9	230	27
#99	26.1	24 h	Re-ReO_2	Outer: Pt/Rh, inner: Pt/Rh	0.03622	0.00092	0.02038	4.98	MgO-NaCl	13	50	30
#100	26.1	24 h	Co-CoO	Outer: Co, inner: Pt/Rh	0.02318	0.00196	0.02332	4.98	MgO-NaCl	8	10	29
#102	26.1	24 h	Ni-NiO	Outer: Ni, inner: Pt/Rh	0.02632	0.00054	0.02336	0.39	MgO-NaCl	7	10	34
#108	26.1	24 h	Ni-NiO	Outer: Ni, inner: Pt/Rh	0.02442	0.00214	0.02520	14.10	MgO-NaCl	10	330	40
#109	26.1	24 h	Ni-NiO	Outer: Ni, inner: Pt/Rh	0.02779	0.00186	0.02253	4.98	MgO-NaCl	12	20	51
					$ThSiO_4$							
#104	26.1	24 h	Co-CoO	Outer: Co, inner: Pt/Rh	0.02361	0.00269*	0.02292	0.39	MgO-NaCl	12	4	43
#105b	26.1	24 h	Re-ReO2	Outer: Pt/Rh, inner: Pt/Rh	0.02372	0.00183*	0.02488	0.39	MgO-NaCl	8	7	43
#107	26.1	24 h	Re-ReO2	Outer: Pt/Rh, inner: Pt/Rh	0.02445	0.00429*	0.02154	14.10	MgO-NaCl	7	10	30
#110	7.1	24 h	Re-ReO2	Outer: Pt/Rh, inner: Pt/Rh	0.02032	0.00257*	0.02865	14.10	MgO-NaCl	6	2	27

Runs indicated by * are Th solubility experiments

using either ¾ inch, pure NaCl assemblies or ½ inch MgO-NaCl assemblies, both with stepped graphite heaters. The temperature was measured by Pt/Pt-Rh ("S-type") thermocouple and monitored by a Eurotherm controller. Friction correction of 0 and 5% were applied for the NaCl and MgO-NaCl assemblies, respectively. Uncertainties in the recorded pressures and temperatures are estimated to be ±1 kbar and ±10°C, respectively. Pressure and temperature was raised simultaneously along a fluid isochoric path. This method and the use of NaCl and MgO-NaCl pressure cells led to minimal deformation of the capsules. NaCl and MgO could completely be removed from the capsules after the experiments; thus the capsules could be precisely weighted after the experiments. No water loss from the

Table 2 Composition of run products

Sample	**Di02**-UO_2 source, Co-CoO buffer, NaCl-free fluid				**Di06-**$ThSiO_4$-source, CoCoO buffer, NaCl-free fluid			
Mineral (nr of analyses)	Diopside(11)	Range	Zoisite(4)	Range	Diopside(4)	Range	Zoisite(2)	
SiO_2	53.6	50.6–55.4	39.7	39.5–39.9	53.1	51.4–53.7	39.1	
Al_2O_3	3.47	1.14–7.56	33.7	33.5–34.0	3.29	2.85–3.95	33.4	
MgO	17.4	16.5–18.6	0.42	0.24–0.63	17.1	16.6–17.7	0.92	
CaO	24.7	23.9–25.4	23.9	23.7–24.16	24.2	23.8–24.5	23.5	
Na_2O	0.00	0.00	0.00	0.00	0.00	0.00	0.00	
Total	99.1		97.7				96.9	
	Average(9)		Average(4)		Average(7)		Average(4)	
U (ppm)	9	28%	1470	58%	10	33%	160	107%
Th (ppm)	3	72%	670	109%	8	25%	430	116%

Sample	**Di03**-UO_2 source, Co-CoO buffer, H_2O + 14.1 wt% NaCl					**Di04**-UO_2 source, Co-CoO buffer, H_2O + 14.1 wt% NaCl			
Mineral (nr of analyses)	Diopside(9)	Range	Garnet(6)	Range	Leuchtenbergite(2)	Diopside(3)	Range	Zoisite(3)	Range
SiO_2	55.1	54.4–55.6	43.2	42.4–44.4	31.7	53.2	52.8–53.8	39.8	39.7–39.9
Al_2O_3	2.30	1.93–2.77	24.0	22.2–24.9	20.1	6.51	5.69–7.23	33.7	33.5–33.9
MgO	17.3	16.9–17.8	20.5	18.1–22.0	33.9	16.0	15.4–16.7	0.51	0.37–0.66
CaO	24.2	23.4–24.9	12.6	10.8–15.86	0.16	23.1	22.2–23.9	24.0	23.9–24.0
Na_2O	0.74	0.35–1.16	0.07	0.00–0.35	0.00	1.04	0.64–1.35	0.02	0.02
total	99.7		100.3		85.8	99.9		98.0	
	Average(9)		Average(3)		Average(2)	Average(10)		Average(4)	
U (ppm)	12	25%	41	26%	0	11	28%	310	28%
Th (ppm)	7	85%	4	29%	0	6	34%	540	146%

Sample	**Di07**-UO_2 source, Re-ReO_2 buffer, H_2O + 14.1 wt% NaCl				Starting powder
Mineral (nr of analyses)	Diopside(7)	Range	Zoisite(2)		
SiO_2	53.7	52.4–54.7	39.2		53.0
Al_2O_3	4.48	3.04–6.77	33.5		5.07
MgO	16.5	15.9–172	0.63		17.8
CaO	23.3	22.6–24.0	23.6		24.1
Na_2O	1.11	0.82–1.34	0.02		
total	99.0		97.0		
	Average(9)		Average(4)		
U (ppm)	14	14%	1200	25%	
Th (ppm)	7	36%	760	53%	

single capsules and from the inner capsules of the buffered experiments was detected.

Synthetic fluid inclusion experiments were carried out at constant temperature of 800°C and pressures of 7.1–26.1 kbars (Table 1). Five synthetic fluid inclusion experiments were conducted without controlling oxygen fugacity at 15 kbars, whereas 17 experiments were conducted at Re-ReO_2, Ni-NiO, Co-CoO or Fe-FeO oxygen fugacity buffers (Table 1). Fluid pH is not explicitly buffered in these experiments, but it is indirectly controlled by the autodissociation of NaCl in the saline fluids, which should produce a slightly alkaline solution. Experimental duration was 1–4 days. The runs were terminated by decreasing the temperature from 800°C to room temperature within ~4 min, resulting in a pressure decrease by about 30%, and subsequently bleeding off the remaining pressure within 15 min. The U and Th solubility experiments in diopside and garnet were quenched by shutting off the power and keeping the pressure constant during cooling. The pressure was lowered to room pressure within 20 min.

Analytical techniques

Quartz pieces of the synthetic fluid inclusion experiments were mounted in epoxy and doubly polished. For analysis, we selected fluid inclusions that did not show any decrepitation phenomena and did not contain optically visible, accidently trapped solid UO_2 or $ThSiO_4$ (i.e., inclusions with constant vapor–liquid–solid ratios). Fluid inclusion analyses were carried out with an Elan quadrupole mass spectrometer (Perkin Elmer) attached to a Geolas M 193 nm ArF ecximer laser (Coherent). NIST SRM 610 glass was used as an external standard. Helium was applied as a carrier glass in the sample chamber. Technical details of the analyses are the same as described by Duc-Tin et al. (2007). Isotopes of ^{23}Na, ^{29}Si, ^{85}Rb, ^{133}Cs, ^{59}Co, ^{238}U or ^{232}Th were analyzed in all run products. ^{57}Fe, ^{60}Ni or ^{185}Re were additionally analyzed in the runs buffered by Fe-FeO, Ni-NiO and Re-ReO_2, respectively, to check for possible contamination of the fluid by these elements. No iron, rhenium or nickel contamination was observed. During the analyses, the laser spot size was increased in several steps so as to pierce the inclusion first with a small beam (typically 6–10 μm), in order to avoid inclusion decrepitation, and finally ablating the whole inclusion volume. The number of fluid inclusions analyzed from a given sample varied from 5 to 23 (Table 1).

Run products for studies of U and Th solubility in silicate minerals were also mounted in epoxy but polished only on one side. Mineral phases were identified by a Jeol Superprobe JXA-8200. Analyses were carried out with an accelerating voltage of 25 kV, a beam current of 20 nA and a beam size of 1–5 microns. Counting time for each element was 30 s. Natural and synthetic standards were used for calibration, and ZAF correction was applied. LA-ICPMS analyses were carried out on the same instrument as for the fluid inclusions. Due to the generally small grain size, the beam diameter was 6–15 microns, and the repetition rate was 5 Hz. The dwell time was 10 ms for Na^{23}, Mg^{25}, Al^{27}, Si^{29} and Ca^{42} but 30 ms for U^{238} and Th^{232}. Besides single crystals, fine grained diopside aggregates were also analyzed. In most cases, the signal in the aggregates was identical with those analyzed in single crystals, it was homogeneous, and no indication of trapped U or Th rich fluid inclusions or grain boundary films was observed (Fig. 3e).

Results

Synthetic fluid inclusions

A large number of primary fluid inclusions formed in quartz overgrowths within 24 h from the start of the experiments. They are rounded or negative crystal shaped and reach sizes of up to 150–200 μm (Fig. 3). A few inclusions formed also in cracks within the original quartz crystal and thus were classified as pseudosecondary. In most experiments, a layer rich in UO_2 or $ThSiO_4$ particles formed at the border between original quartz and new quartz overgrowth (e.g., lower right of Fig. 3c). Fluid inclusions close to this layer could not be analyzed due to the risk of simultaneously ablating such particles.

Unbuffered experiments

The uranium content of fluid inclusions analyzed from fO_2-unbuffered experiments shows a large variability at all fluid salinities investigated (Table 1; Fig. 4a). In almost pure H_2O fluid (0.20 wt% $NaCl_{equiv}$), U concentrations range from 10 to 160 ppm, in 14.10 wt% $NaCl_{equiv}$ fluid from 90 to 1,190 ppm, and in 41.73 wt% $NaCl_{equiv}$ fluid from 520 to 1,810 ppm (Fig. 4a). Thus, U solubility seemed to increase with increasing fluid salinity, but exact predictions could not be made due to the large scatter.

Variations in the U content of fluid inclusions from one single experiment can be caused by two main processes: (1) fluid that is trapped very early, before equilibrium with respect to UO_2 (or $ThSiO_4$) is reached, will show artificially low concentrations; (2) changes in the oxygen fugacity can lead to changes in U solubility. In order to check which of these two effects was dominant in our experiments, we added known amounts of Co (582–955 ppm) to the fluid. Because Co alloys with the Pt/Rh capsule during the experiment, its concentration in the fluid should decrease with increasing run time. The Co content of fluid inclusions can thus be used to put the inclusions into relative entrapment sequence. Figure 4b shows the variation of the U content of fluid inclusions from experiments #74 as a function of their Co content and compares them with the results obtained from Re-ReO_2-buffered experiment #84. Both experiments were carried out at the same salinity of 14.10 wt% $NaCl_{equiv}$. A clear decrease in the U content is observed with decreasing Co content in the unbuffered run #74, suggesting that fO_2 in the capsule decreased over time. In contrast, the U concentration in the fluid of run #84 shows no systematic variation over the entire range of 400–900 ppm Co, implying that equilibrium with respect to the fO_2 buffer was reached very quickly. These experiments demonstrate that it is crucial to buffer fO_2 conditions in solubility studies in which the element of interest may attain different valance states.

Experiments with fO_2 buffers

Two U solubility experiments with iron-wustite buffer were carried out with fluids containing 0.39 and 14.1 wt% $NaCl_{equiv}$, respectively (Table 1). U concentrations in the

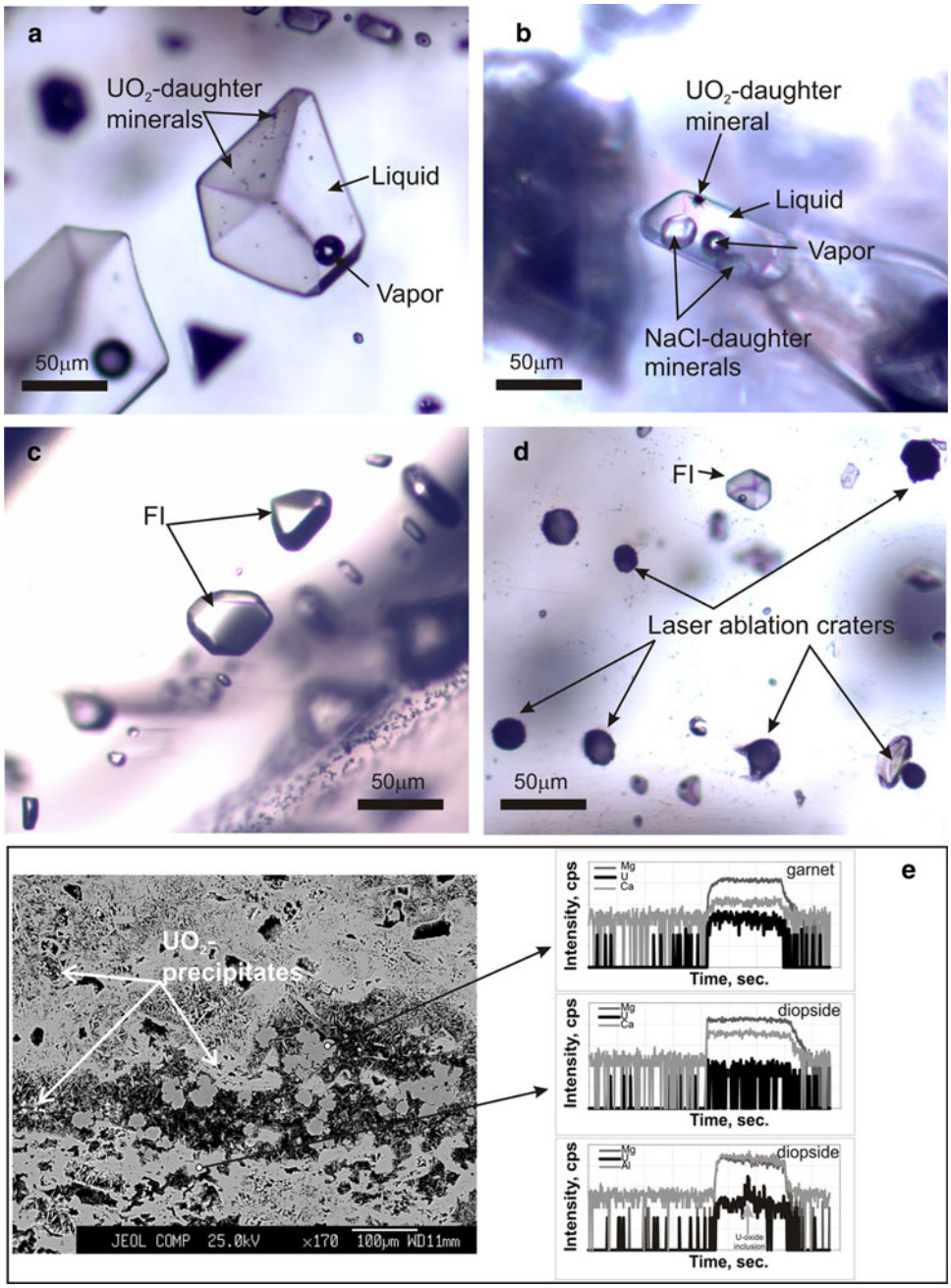

Fig. 3 Photomicrographs of synthetic fluid inclusions (FI) in quartz. **a** Negative crystal-shaped FIs containing a vapor bubble, a liquid phase and UO_2 precipitates (daughter minerals). The fluid contains 14.10 wt% $NaCl_{equiv}$ and was trapped at 15 kbar and 800°C (Run 74). **b** Negative crystal-shaped FIs containing a vapor bubble, a liquid phase, UO_2 and NaCl precipitates (daughter minerals). The fluid contains 41.73 wt% $NaCl_{equiv}$ and was trapped at 15 kbar and 800°C (Run 75). **c** Negative crystal-shaped FIs trapped at 26.1 kbars, 800°C from fluid containing 14.10 wt% $NaCl_{equiv}$. Note the lack of vapor bubbles due to the >1.0 g/cm^3 fluid density at these conditions (Run 84). **d** Laser ablation pits and one unopened fluid inclusion close to the sample surface (Run 74). **e** Back scattered electron image of sample Di03, containing diopside, garnet and UO_2 precipitates (26.1 kbar, 800°C, CoCoO buffer, 14.1 wt% $NaCl_{equiv}$ salinity). *White dots* are indicating the sites of La-ICP-MS analyses. Respective schematic LA-ICPMS spectra are shown in the *left*. Only homogeneous garnet and diopside spectra were integrated. Spectra showing the signs of UO_2 precipitates (lowermost spectrum) were not calculated

inclusions were always below the detection limit, so Table 2 and Fig. 5a and c report only the lowest detection limit we obtained.

Three U solubility experiments were conducted with each of the other fO_2 buffers at 26.1 kbar and 800°C (Fig. 5d–f). At conditions buffered by Co-CoO, U solubility increased from 7 to 230 ppm as the fluid salinity increased from 0.39 to 14.10 wt% $NaCl_{equiv}$ (Table 1; Fig. 5f). A similar increase in U concentration with increasing fluid salinity was observed when the fO_2 conditions were buffered by Ni-NiO (10–320 ppm) and Re-ReO_2 (20–960 ppm) (Fig. 5d, e). Thus, U solubility increased with increasing fluid salinity at all fO_2 studied. At fO_2 conditions buffered between Co-CoO and Re-ReO_2, the effect of increasing fluid salinity from 0.39 to 14.10 wt% $NaCl_{equiv}$ is about twice as strong as the effect of changing the oxidation conditions (Fig. 5). If the results at the Fe-FeO buffer are included, however, the effect of changing fO_2 is at least as strong as the change in fluid salinity. All experimental data on U solubility in fO_2 conditions above Fe-FeO-buffer at 26.1 kbar and 800°C can be described by the equation:

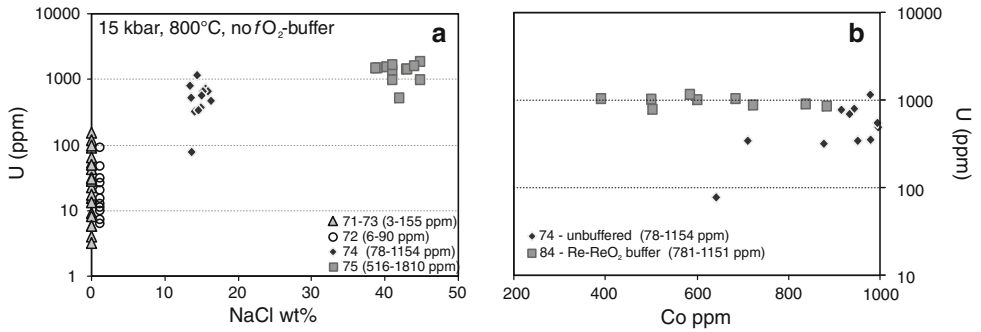

Fig. 4 U content of individual fluid inclusions analyzed from runs 71–75 (without fO_2 buffer) and run 84 (Re-ReO_2 buffer). **a** Fluid salinity versus U content in the experiments without fO_2 control. Note the large spread of U concentrations observed in inclusions from a given run, particularly at low fluid salinities. The small spread in NaCl concentrations arises from the fact that fluid inclusion concentrations were calculated based on Cs as internal standard. **b** Cobalt versus uranium concentrations in fluid inclusions of run 74 (no fO_2 buffering) and of run 84 (fO_2 buffered by Re-ReO_2). The starting concentration of Co in the fluid of both runs was 858 ppm, and it is expected that this concentration decreased with increasing time due to alloying of Co with the $Pt_{95}Rh_{05}$ capsule. Hence, the fact that Co correlates positively with U in experiment 74 suggests that U solubility decreased with increasing time, probably due to decreasing fO_2 in this unbuffered experiment. In contrast, in the Re-ReO_2 buffered experiment 84 the U solubility stayed constant despite a more than twofold decrease in the Co concentration in the fluid

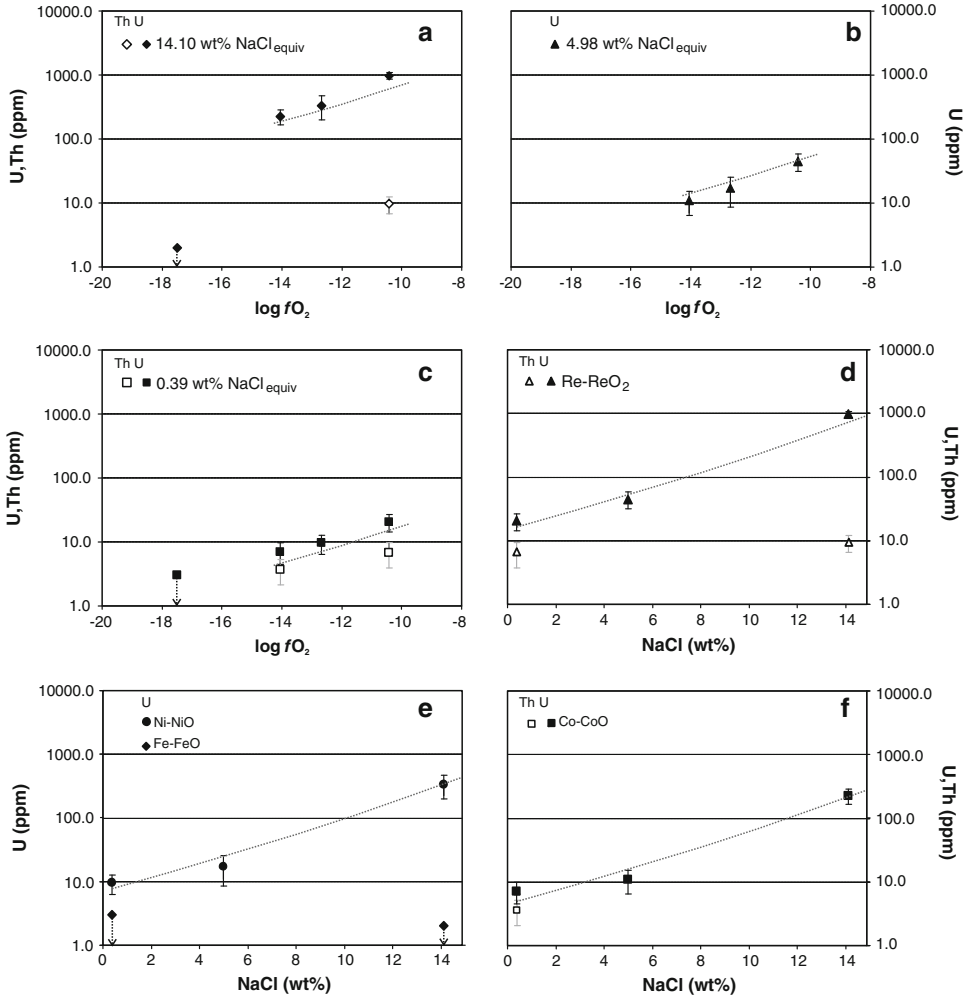

Fig. 5 Variation of U and Th solubility as a function of fO_2 (**a–c**) and fluid salinity (**d–f**) at 800°C and 26.1 kbar. For the Fe-FeO buffer, only a detection limit can be plotted. Oxygen fugacities were calculated using the equations in Frost (1991); Pownceby and O'Neill (1994); Campbell et al. (2006). *Dotted curves* are predicted U solubilities by equation described in the text

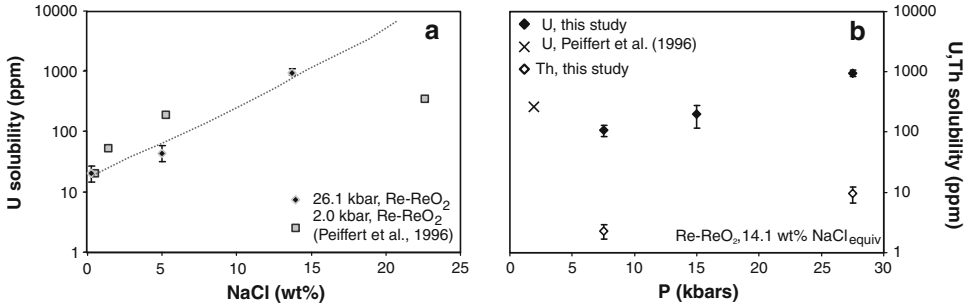

Fig. 6 Dependence of U and Th solubility on pressure and fluid composition. **a** Variation of U solubility with changing fluid salinity at 2 and 26.1 kbars, 800°C and the oxygen fugacity of the Re-ReO_2 buffer. Values at 2 kbars are calculated based on equations in Peiffert et al. (1996). *Dotted curve* is predicted U solubility by equation described in the text for 26.1 kbar. **b** Pressure dependence of U- and Th solubility at 800°C. The data point at 2 kbar is the estimated U solubility in a fluid of the same salinity and the same fO_2 based on the data presented in Peiffert et al. (1996)

$$\log U = 2.681 + 0.1433 \log fO_2 + 0.594Cl$$

where U is uranium solubility (in ppm), fO_2 is oxygen fugacity and Cl is the molality of dissolved chlorine in the fluid. This expression generally reproduces the measured uranium solubilities within analytical error (Figs. 5, 6).

The experimental data suggest that uranium is dissolved in the fluid as a mixture of U^{4+} and U^{6+} species. For a simple oxidation reaction from U^{4+} to U^{6+} such as

$$UO_2 + {}^1/_2O_2 + 2Cl^- + H_2O = UO_2Cl_2 + 2OH^-$$

One would expect an increase in uranium solubility with the square root of oxygen fugacity. The exponent of 0.1433 of the oxygen fugacity observed implies that both U^{4+} and U^{6+} coexist in the solution. At very low oxygen fugacity, where only U^{4+} is stable, the dependence on oxygen fugacity should level off. Our data suggest that this will happen only below the Fe-FeO buffer. The exponential increase with Cl concentration implies that the ratio of UO_2^{2+} to Cl^- in the species of hexavalent uranium changes with salinity, possibly from UO_2^{2+} through UO_2Cl^+ to UO_2Cl_2. This is consistent with the study by Peiffert et al. (1996) who also concluded that several species of uranium with different oxidation state and different Cl/U ratio coexist in the fluid in equilibrium with UO_2 at 2 kbar.

Compared to uranium, the solubility of Th changes very little with fluid salinity and seems to be also less dependent on fO_2, although the latter is not certain due to the relatively large error bars (Table 1; Fig. 5). Thorium solubility in fluid with 0.39 wt% $NaCl_{equiv}$ increased from 4 ± 2 to 7 ± 3 ppm when fO_2 changed from the Co-CoO to the Re-ReO_2 buffer (Table 1; Fig. 5). At conditions buffered by Re-ReO_2, thorium solubility increased from 7 ± 3 to 10 ± 3 ppm when the fluid salinity changed from 0.39 to 14.10 wt% $NaCl_{equiv}$ (Table 1; Fig. 5). Importantly, Th is significantly less soluble than U at all conditions studied, with the largest difference (more than 2 orders of magnitude) occurring at the highest fluid salinity.

Effect of pressure on U and Th solubility

The relationship between U solubility, fO_2 conditions and fluid salinity has been studied at 2 kbars and 770°C by Peiffert et al. (1996). The expected solubilities at 2 kbar and 770°C are similar to our data for the lowest fluid salinity (0.1 M NaCl) and for fO_2 between Co-CoO and Re-ReO_2 (Fig. 6, only Re-ReO_2 is shown). For higher fluid salinities, the predicted low-pressure solubilities differ from those observed in this study by up to 1 order of magnitude, and at Fe-FeO buffered conditions by more than 1.5 orders of magnitude.

Since the experiments of Peiffert et al. (1996) were performed at almost the same temperature as ours (770 vs. 800°C) we consider it unlikely that temperature differences caused this discrepancy. The experiments of e.g., Zharikov et al. (1987) and the theoretical work of Shock et al. (1997) suggest that a temperature difference of 30°C at this high-temperature region does not lead to a significant change in U solubility. The large pressure difference between our study and that of Peiffert et al. (1996) might be a more likely explanation for the observed discrepancies.

Figure 6a shows the relationship between U solubility, fluid salinity and pressure in the combined dataset. At 2-kbars pressure Peiffert et al. (1996), the solubility of U increases strongly with increasing fluid salinity up to a NaCl content of 5 wt%, above which value the U concentration stays almost constant (Fig. 6a). In contrast, at 26.1-kbars pressure the solubility of U increases more strongly at high fluid salinities than at low fluid salinities (Fig. 6a). The explanation for this difference is that the stability of metal-chloride complexes depends on the number of available Cl^- anions rather than on the total amount of chloride present in the system (Eugster 1986). NaCl dissolves in aqueous solutions mainly in the form of molecular NaCl at low pressures (particularly at high fluid salinities), whereas above ~10 kbars it completely dissociates into Na^+ and Cl^- (e.g., Quist and Marshall 1968;

Aranovich and Newton 1996, and references therein). Thus, at low pressures the amount of free Cl^- anions is limited. In contrast, at high pressures the number of available Cl^- anions should be proportional to the fluid salinity.

The effect of increasing pressure on the solubility of U and Th in a fluid of constant salinity (14.10 wt% $NaCl_{equiv}$) is shown in Fig. 6b. Between 7.1 and 26.1 kbars, the solubility of U increases by almost one order of magnitude, whereas that of Th increases by a factor of 5. It is noted that U solubility increases more strongly between 14.3 and 26.1 kbar than between 7.1 and 14.3 kbar, despite the fact that NaCl should be already completely dissociated at 14.3 kbar. This suggests that the increase in U (and Th) solubility at high pressure cannot depend exclusively on the available Cl^- anions.

In general, our data, combined with the results of Peiffert et al. (1996), suggest that the effect of pressure on uranium and thorium solubility is of only secondary importance when compared to oxygen fugacity and salinity. The solvent properties of a fluid are primarily controlled by density, which in turn controls the dielectric constant. The density of water at 2 kbar and 770°C is 0.45 g/cm^3, while it is 1.14 g/cm^3 at 800°C and 26.1 kbar. As noted above, this variation in density changes uranium solubility by a maximum of 1.5 orders of magnitude. A further increase in pressure up to 40 kbar (corresponding to the average depth of the subducted slab below the volcanic front) will only slightly increase fluid density ($\sim$1.25 g/cm^3) and should therefore have only a minor effect on solubilities. Moreover, as both uranium and thorium solubility increase with pressure, the effect of increasing pressure from 26.1 to 40 kbar on U/Th fractionation is likely to be negligible.

Solubility of U and Th in diopside, zoisite and garnet

The solubility of U and Th in diopside and pyrope-rich garnet was determined in equilibrium with uraninite and thorite. After 48 h, diopside and zoisite crystals have developed in most runs (Table 2). In one of the runs pyrope-rich garnet, diopside and a leuchtenbergite (Fe-free chlorite) formed, probably due to a slight heterogeneity in the loaded starting powder. Microprobe analyses showed that with exception of the Al-content in diopside, the major element composition of all phases was homogeneous in the whole capsule (Table 2). The Al_2O_3 content of diopside varied between 1.1 and 7.6 wt% in all run products (Table 2). Th and U were found both in the samples buffered by uraninite and in those buffered by thorite, because the natural uraninite used contained some Th and the thorite contained some U. The observation that the uranium and thorium contents observed in equilibrium with thorite were often similar to those in equilibrium with uraninite may imply that some unmixing of the solid solutions occurred during the experiment, e.g., the $(U,Th)O_2$ solution may have reacted to nearly pure UO_2 and $ThSiO_4$. Because of the small fraction of these minerals used, this could not be verified after the run.

In all experiments where zoisite was present, it was the major silicate phase, which incorporated U and Th. U and Th concentrations were highly variable in zoisites in single run products (Table 2). Despite this variation, it is obvious that in the run buffered by $ThSiO_4$ Th concentrations were higher, whereas in those with uraninite, U was higher in zoisites.

The average U content in diopside in equilibrium with both thorite and uraninite was $\sim$11 ppm independently of fluid salinity, coexisting mineral phases and fO_2 conditions. This latter observation is in accordance with the previous results, showing that uranium can be incorporated dominantly as U^{4+} to the M2 site of clinopyroxene, as the ionic radii of higher charged U^{5+} and U^{6+} cations are too large compared to the radius of M1 site and too small to be incorporated to the M2 site (Hill et al. 2000). In contrast to ziosite, Th concentration in diopside in equilibrium with thorite or uraninite agreed well within the uncertainty of the analyses (Table 2). There was no obvious dependence of U and Th concentrations on the Al_2O_3-content of diopsides; however, this dependence may be hidden due to the relatively large uncertainties in the U and Th data. Moreover, Lundström et al. (1998) demonstrated that while small concentrations of Al have a strong effect on the partitioning of Th between melt and clinopyroxene, this effect levels off at Al_2O_3 contents higher than 3 wt%.

Pyrope-rich garnet formed only in one run product in the presence of uraninite. The average U content was 41 ppm, whereas the concentration of Th in the analyzed grains was approximately 10 times less (Table 2). Although this run cannot be regarded as being saturated in Th, this U/Th ratio agrees well with the previously observed U-Th fractionation in pyrope-rich garnets (Brenan et al. 1995; Kessel et al. 2005) in equilibrium with aqueous fluid.

In all the analyzed chlorite grains, both U and Th were below detection limit.

Partitioning of U and Th between fluid and silicate phases

The partitioning of U between aqueous fluid and minerals can be calculated as the ratio of the UO_2 solubility in the fluid to the UO_2 solubility in the mineral. Thorium solubility can be calculated in the same way from the experiments saturated with $ThSiO_4$. The fact that two different standard states were used for uranium and thorium cancels out in this calculation, if all other physical conditions of the experiments are the same. This is because an increase in chemical potential of U or Th in the standard state would cause a

proportional increase in U or Th solubility in both fluid and mineral, as long as Henry′s law if fulfilled. Although the major element composition of aqueous fluid in equilibrium with a diopside + zoisite or diopside + garnet assemblage might be not exactly the same as in fluids equilibrated with quartz, the solute content of the fluid should be silica dominated in both cases (e.g., Newton and Manning 2008; Manning 2004; Kessel et al. 2005 etc.). It was shown above that it is the Cl^- concentration rather than the silica content that controls the solubility of U in the fluid. Thus, the mineral–fluid partition coefficients calculated from our experiments should approach the real values. Moreover, fluid/melt partitioning experiments of U at 2 kbar, carried out in complex, alkali and aluminosilicate-containing systems (Keppler and Wyllie 1990, 1991), agree well with predictions from solubility data for UO_2 as measured in an Al-free system (Peiffert et al. 1996). This implies that the presence of some Al in the system will not fundamentally change the behavior of U (and by inference, of Th).

A potential problem in our calculation is, however, the effect of silica activity on the solubility of thorite $ThSiO_4$. Since thorite contains SiO_2, its solubility must depend on silica activity. However, silica activity buffered by olivine and enstatite (as in the mantle) is approximately 0.6 as opposed to the silica activity of 1 as buffered by quartz in some of our experiments, and silica activity in the remaining experiments was probably between quartz and olivine saturation. This would translate into a change of thorite solubility by a maximum factor of 1.7. This is negligible if compared to the orders of magnitude fractionation of U relative to Th as induced by variations in oxygen fugacity and fluid salinity.

Figure 7a–c shows the variation of U and Th partitioning between fluid and diopside or pyrope. Uranium partitions into the fluid phase at elevated fluid salinities with respect to both diopside and garnet. Moreover, at oxidation conditions above the FMQ buffer $D_U^{fluid/cpx}$ is above unity. This agrees well with the observation of Brenan et al. (1995). $D_U^{fluid/cpx}$ decreases at all fluid salinities approaching more reducing conditions. Decreasing fluid salinity also leads to the decrease in $D_U^{fluid/cpx}$. In case of garnet, the same relationships with fO_2 conditions and fluid salinity

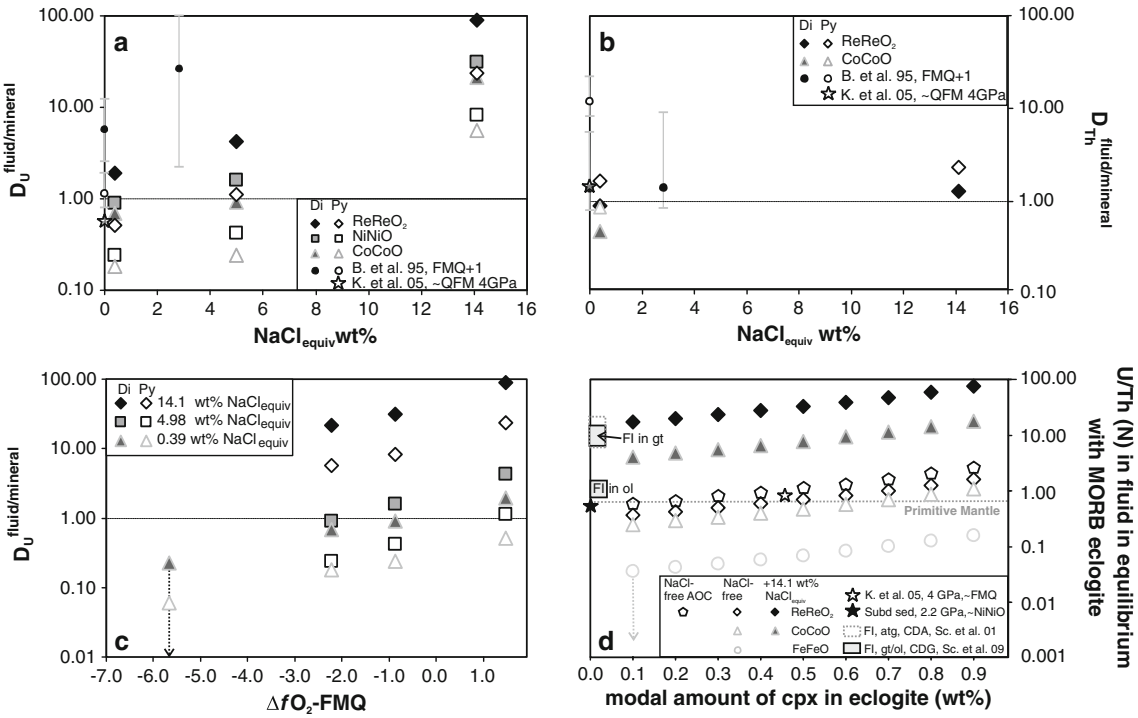

Fig. 7 Partition coefficients of U and Th between diopside (Di), pyrope (Py) and aqueous fluid as a function of fluid salinity (**a**, **b**) and fO_2 (**c**) at 26.1 kbar and 800°C. The partition coefficients for U at oxidation conditions buffered by Iron-Wustite in (**c**) are minimum values, as the U concentration in the fluid was below detection limit. Partition coefficients determined by Brenan et al. (1995) and Kessel et al. (2005) are also shown for comparison. **d** Shows the composition of aqueous fluid in equilibrium with N-MORB (Hart et al. 1999) and altered MORB (Jochum and Verma 1986) eclogite at variable oxidation conditions and fluid salinities, as a function of the clinopyroxene/garnet ratio in the eclogite. Fluid compositions were calculated assuming only clinopyroxene and garnet present as solid phases. For comparison, the following fluid compositions are plotted: Kessel et al. (2005); calculated fluid composition in equilibrium with subducted sediment using bulk partition coefficients of Spandler et al. (2006) and subducted sediment composition of Plank and Langmuir (1998); and natural fluid inclusion compositions in high pressure harzburgites from Cerro del Almirez (CDA) (Scambelluri et al. 2001) and Cima di Gagnione (CDG) (Scambelluri et al. 2009; Pettke personal communication)

can be observed. Moreover, U becomes compatible in garnet at fluid salinities below 5 wt% $NaCl_{equiv}$, which is in accordance with the experimental data of Brenan et al. (1995) and Kessel et al. (2005). In terms of Th partitioning, no apparent change is observed with any of the studied variables as the solubility of Th in both fluid phase and silicate minerals seems to be independent of fluid salinity and fO_2 conditions. The U and Th partition coefficients calculated from our experiments agree well within the uncertainty range of the previously published values verifying the applicability of our method.

Implications for U-Th decoupling in subduction zones

Fluid compositions

Our experiments suggest that oxygen fugacity and salinity together are the dominant variables that control U/Th fractionation in subduction zone fluids. The fractionation is likely to be due to the stabilization of chlorine complexes of the UO_2^{2+} cation containing hexavalent uranium. Indeed, a theoretical study of the relative stability of various thorium and uranium containing complexes in high-density aqueous fluids (Bailey and Ragnasdottir 1994) failed to detect any complexes or ligands that would produce a fractionation of uranium from thorium comparable to that observed here in Cl-bearing oxidized fluids. In addition to chlorine, high-density fluids may contain various silicate and aluminosilicate anions that may interact with uranium and thorium. However, these anions occur in highest concentration in silicate melts, and a fractionation of uranium and thorium between melt and crystals that would strongly enrich uranium in the melt has never been observed. Therefore, the possibility that U may be fractionated from Th by silicate or alumosilicate ions in the fluid can be discounted. We therefore focus here on the effect of oxidation state and salinity of subduction zone fluids on the decoupling of uranium and thorium.

Figure 7d shows the calculated U/Th(N) ratio of aqueous fluids in equilibrium with fresh and altered MORB eclogite (Hart et al. 1999; Jochum and Verma 1986, respectively). These values were calculated by assuming that only garnet and clinopyroxene are present in the eclogitic assemblage. The enrichment of U over Th in the fluid phase increases if the modal amount of clinopyroxene in the eclogite increases. The fluid phase in equilibrium with fresh MORB eclogite is enriched in U over Th compared to primitive mantle (McDonough and Sun 1995) under oxidized conditions if the fluid contains significant amount of chlorine. In Cl^--free fluids, and fO_2 conditions between Co-CoO and Re-ReO_2, U enrichment over Th only occurs if the eclogite is clinopyroxene rich. The relationship is similar for fluids in equilibrium with altered MORB. As altered oceanic crust can be significantly enriched in both U and Th relative to fresh N-MORB, the fluid phase in equilibrium with altered MORB eclogite will show only slightly higher U/Th(N) ratios compared to that in equilibrium with fresh MORB. In strongly reducing conditions, buffered by iron-wustite, the fluid phase should always be enriched in Th over U. The plotted values should be regarded as maximum values, as the exact partition coefficients for U could not be determined at these reducing conditions. Methane and graphite-bearing fluid inclusions have been reported from mafic rocks and sediments subducted to different depths (e.g.: Sakaguchi 1999; Liu and Fei 2006) and from mantle wedge peridotites (Song et al. 2009), showing that strongly reduced fluids are locally present in the mantle. Most studies, however, suggest that such reducing conditions are not dominant in arc magmas and their source regions (e.g.: Parkinson and Arculus 1999; McInnes et al. 2001; Lee et al. 2005; Ishimaru et al. 2007, etc.).

Figure 7d also shows the U/Th(N) ratios of aqueous fluid in equilibrium with the eclogitic assemblage of Kessel et al. (2005) and in equilibrium with subducted sediments. Later value was calculated using the subducted sediment bulk composition of Plank and Langmuir (1998) and the bulk partition coefficients of Spandler et al. (2006). In all these experiments, the fluid was Cl^- free. The fluid compositions from both assemblages agree well with our predicted values and confirm that Cl^--free fluid will not be significantly enriched in U relative to Th in these environments.

Figure 7d furthermore shows the U/Th(N) ratios measured in natural fluid inclusions in olivines and garnets from Cerro del Almirez and Cima di Gagnione harzburgites (Scambelluri et al. 2001, 2009, Pettke personal communication). The U/Th(N) ratios cover a wide range in those inclusions. The determination of fluid salinity in this type of fluid inclusions is difficult, because of the likelihood of post-entrapment water loss. Based on mass balance considerations, Scambelluri et al. (2004a) suggest that the salinity in the inclusions in harzburgites is relatively low, between 0.4 and 2 wt% $NaCl_{equiv}$. If this is true, then their measured U/Th(N) ratios are surprisingly high. One explanation could be that these rocks were equilibrated at much higher fO_2 conditions than those are covered by our experiments. Another explanation might be that the inclusions were trapped in the ultramafic segment of the subducted slab, thus the fluid, evolved in equilibrium with mineral assemblages (serpentine → olivine + antigorite → garnet + orthopyroxene + chlorite) that are different from the mineral association in our model calculation.

Our estimates of fluid composition are based on experimental data obtained at 800°C and 26.1 kbar, which is

reasonably close to expected conditions for amphibole dehydration during the amphibolite to eclogite transition. Although the temperature dependence of U and Th solubility has not been explicitly studied, one can reasonably assume that it will be similar to that of other high-field strength elements. Audetat and Keppler (2005) obtained an enthalpy for the dissolution of rutile in water of 74.7 kJ/mol, which would correspond to an approximate doubling of solubility upon an increase of temperature by 100°C. If the temperature dependence of uraninite and thorite solubility in aqueous fluids is similar, this means that variations in temperature will be only of secondary importance when compared to variations in oxygen fugacity and salinity. Moreover, the U/Th ratio in the fluid will remain unchanged if uraninite and thorite solubilities respond in a similar way to temperature changes. This would be consistent with the observation made in this study that both thorite and uraninite solubilities increase with pressure and with a similar slope (Fig. 6b).

Preservation of U/Th ratio of slab fluids during passage in the mantle wedge

In order to preserve a specific U/Th ratio and bulk U and Th concentrations in slab fluids during their passage through the overlying mantle wedge, the fluid/mineral partition coefficients in the mantle wedge have to be larger or of comparable value as in the slab. Alternatively, the U and Th content may also remain constant if the fluid flow is mostly channeled, with only a small volume of peridotite approaching chemical equilibrium with the fluid. Compared to clinopyroxene and garnet, orthopyroxene and olivine incorporate orders of magnitude less U and Th into their structure (e.g., Wood et al. 1999). Thus, olivine and orthopyroxene play only a limited role in changing the U/Th ratios in coexisting melts or fluids. Wood et al. (1999) have shown that the partitioning behavior of U^{4+} and Th^{4+} between silicate melt and clinopyroxene changes with pressure and temperature owing to the change in the M2 site radius of clinopyroxene. They have demonstrated by both theoretical calculations and experiments that if the radius of M2 site decreases below 1 Å, the partition coefficients of U between clinopyroxene and melt will be higher than that of Th. Thus, U^{4+} will be more compatible in clinopyroxene than Th^{4+} during mantle melting. This happens only in clinopyroxenes with significant Al_2O_3 contents (above approx. 11 wt%). However, clinopyroxenes in upper mantle xenoliths and peridotite massifs generally contain much less Al_2O_3 (<9 wt%). All of these mean if aqueous fluid is liberated from the subducted slab with a high U/Th(N) ratio, it can preserve its composition during its passage through the mantle wedge in spinel peridotite stability field.

High U/Th(N) ratios should also be preserved in garnet peridotite stability field if the clinopyroxene/garnet ratio is higher than 1 or if the fluid is at least moderately saline ($\geq$5 wt% $NaCl_{equiv}$) (Fig. 7d). Serpentine has the capacity to carry significant chlorine (e.g., Scambelluri et al. 2004b; Sharp and Barnes 2004) to great depth during subduction, leading to the liberation of variably saline fluid during its continuous dehydration. The stability of antigorite depends on the thermal structure of the subducted slab. According to Schmidt and Poli (1998), it can be a stable phase down to more than 200 kms depth, allowing a continuous fluid flux from the slab into the overlying mantle wedge. Although the Cl^- content of released fluids might decrease with increasing depth (Scambelluri et al. 2004a, b), it might have the capacity to carry an elevated amount of U relative to Th to the source region of arc magmas. Beyond antigorite stability, hypersaline fluids are less significant (Scambelluri et al. 1997).

Composition of arc magmas

From our experimental data, we calculated the U/Th(N) ratio of arc magmas that have absorbed various amounts of aqueous fluids with different salinity that were equilibrated with a MORB eclogite at oxidizing and reducing conditions. The results of this calculation are shown in Fig. 8 as a function of the La/Yb ratio, which is a proxy of the degree of melting (with low degree partial melts producing high La/Yb). Implicit assumptions in this calculation are (1) that the fluid contribution to the La and Yb budget is negligible and (2) that the U and Th concentrations of the fluids released from the subducted slab were not much altered during passage through the mantle wedge. Hypothetical partial melts of dry 4-phase spinel and garnet lherzolites (with primitive mantle bulk composition of McDonough and Sun 1995) were calculated based on the melting reactions of Kinzler and Grove (1992) and Walter (1998), partition coefficients of Salters et al. (2002) and McKenzie and O'Nions (1991) and equations for non-modal fractional partial melting.

Silicate melt inclusions studied in primitive arc magmas commonly contain up to about 5 wt% H_2O (e.g.: Cervantes and Wallace 2003; Wallace 2005; Gurenko et al. 2005; Benjamin et al. 2007; Shaw et al. 2008), rarely this value can reach up to 10 wt% (Grove et al. 2002). The Cl/H_2O ratio in these melt inclusions also gives some approximate indication of the salinity of the fluids absorbed during magma production (Table 3). Figure 8 shows how 5–10 wt% dissolved aqueous fluid changes the U/Th(N) ratios of the melt compared to those of dry spinel or garnet peridotite partial melts. Cl-free fluid cannot change significantly the melt composition, as it is too dilute in both U and Th at any studied fO_2 conditions. Similarly, the

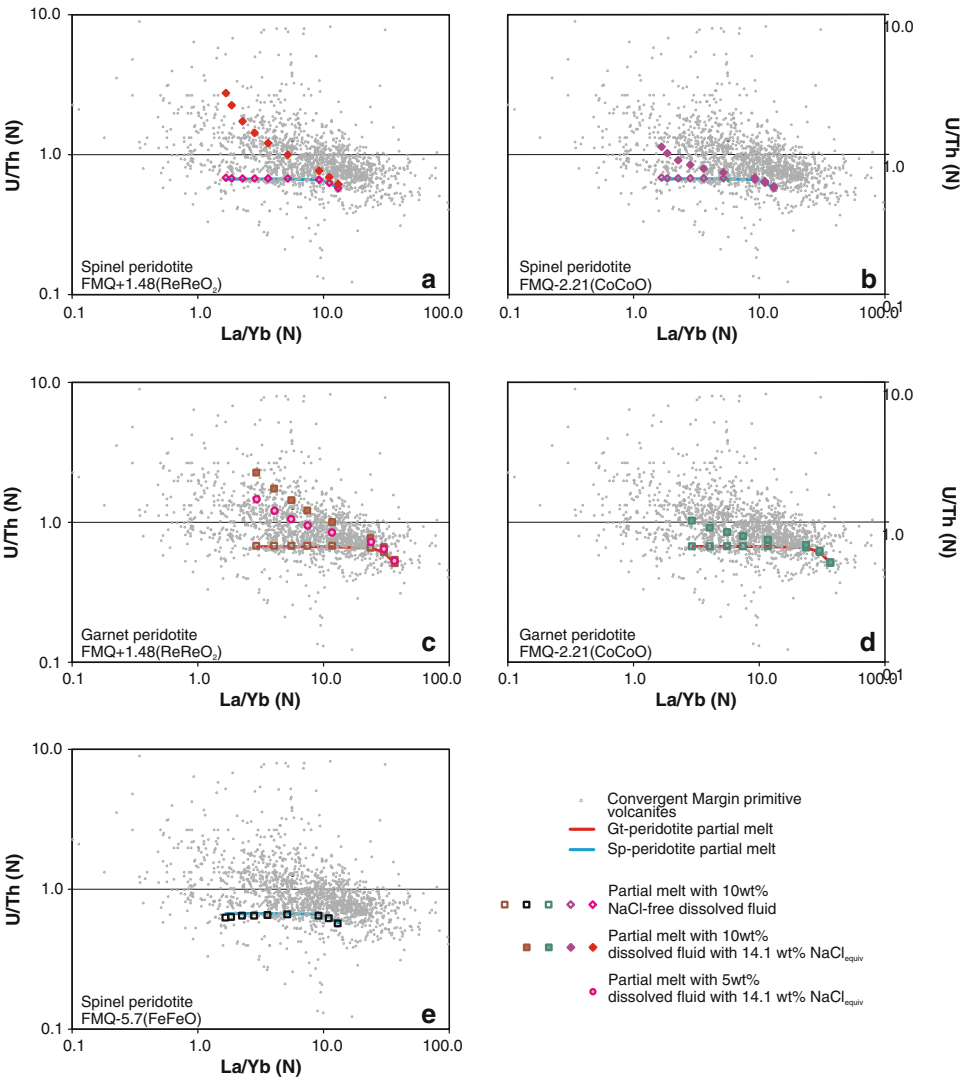

Fig. 8 Distribution of MORB-normalized (Hart et al. 1999) U/Th and La/Yb ratios in primitive basalts from convergent margins compared to dry partial melts of spinel (**a**, **b**, **e**) and garnet (**c**, **d**) lherzolites (as described in Fig. 1) and partial melts containing 5–10 wt% of dissolved aqueous fluid with different salinities and oxidation conditions. A fluid composition in equilibrium with MORB eclogite having a clinopyroxene:garnet ratios of 60:40 was used for this calculation (Fig. 7d). Note that Cl-free fluid is too dilute to change the melt compositions, whereas saline fluid has the capacity to increase the U/Th(N) of the melt even at relatively reducing conditions (FMQ-2.21). Data source is the Georock database at http://georoc.mpch-mainz.gwdg.de/georoc/. Number of plotted melt compositions is 1,740 after filtering as described in Fig. 1

contribution of strongly reduced fluid will not lead to significant enrichment of Th over U in the melt, as the absolute Th content of the fluid is very low. In contrast, if the dissolved fluid is moderately saline, it might significantly increase the U/Th(N) ratio of the melt even at moderate oxygen fugacities. This is in accordance with the Cl^- contents of undegassed olivine-hosted silicate melt inclusions (Table 3), and the results of Kent et al. (2002) who suggested that subduction-related fluids should contain chlorine on a weight percent level, in order to explain the H_2O-K_2O-Cl systematics observed in arc and back arc lavas.

Calculated U/Th(N) ratios in silicate melts containing 5–50 wt% of dissolved saline aqueous fluid are plotted in each figure of Appendix 1, where the primitive melt compositions of 27 subduction-related settings are presented. Compared to previous models (compilation of e.g., Hakesworth et al. 1997), we can now estimate more precisely both the amount of fluid dissolved in silicate melt and the salinity of the dissolved fluid. For example, in case of the primitive volcanics from Sunda arc, Turner and Foden (2001) suggest a significant (10–20%) dissolved aqueous fluid component in the silicate melt based on U/Th vs Sr-isotopic systematics. Our calculations suggest that this dissolved fluid phase should have had low salinity if it has contributed in that significant amount at all. The U/Th(N) ratios and corresponding La/Yb(N) values in e.g., the Izu-Bonin-Mariana, Tonga, Luzon, Kamchatka or the Central American volcanic arc magmas are consistent with 0–10 wt% dissolved saline fluid in the melt formed by the variable degree of partial melting of primitive or MORB mantle source (e.g., Stolper and Newman 1994; Ewart and Hawkesworth 1987; Kamenetsky et al. 1997; Dorendorf et al. 2000; Portnyagin et al. 2007). In contrast, e.g., in the Andean, Honshu or Mexican arcs, variable U/Th(N) ratios correspond even to relatively high La/Yb(N). At low-degree partial melting, which is responsible for the high La/Yb(N) ratios, the absolute U and Th concentrations in

Table 3 Water and Cl^- contents of undegassed, olivine-hosted silicate melt inclusions form the Aeolian and Central American Volcanic Arcs

	wt% H_2O	wt% Cl	Cl^- wt% in fluid	$NaCl_{equiv}$ in fluid
Aeolian arc (32)	3.0–3.6	0.134–0.252	3.9–7.7	6.4–12.7
Central American Volcanic Arc (9)	3.0–5.2	0.080–0.196	2.2–6.1	3.6–10.1

Columns 4 and 5 contain the assumed Cl^- and NaCl contents of the fluid absorbed in the silicate melt. Data sources: Bertagnini et al. (2003), Metrich et al. (2004), Spilliaert et al. (2006) and Corsaro et al. (2009) for Aeolian Arc and Cervantes et al. (2003) and Roggensack et al. (1997) for the Central American Volcanic Arc. Numbers in parenthesis are the number of silicate melt inclusions used for this calculation

the dry melt are high enough, not to be affected significantly by any dissolved fluid phase. The explanation for this variability is the strongly heterogeneous mantle source in terms of U/Th ratios, e.g., different degree of source enrichment by both aqueous fluid and sediment melt, the latter being responsible for the enrichment in Th (e.g., Hickey-Vargas et al. 2002; Cervantes and Wallace 2003; Le Voyer et al. 2008).

There are relatively few melt compositions (e.g., at Ryukyu, Honshu, Cascades or Greater Antilles) in which the U/Th(N) ratios are too high to be explained by the effect of 10 wt% dissolved, moderately saline, aqueous fluid. These melt compositions require either an unrealistically high amount of fluid (up to 50 wt%) or alternatively a fluid phase that had a significantly higher salinity than was covered by our experiments. The very scarce presence of these melt compositions confirms that hypersaline brines play only a limited role in the mantle (Scambelluri et al. 2004a; Kent et al. 2002).

Our experimental data also allow evaluating the proposal that variable U/Th ratios may be produced by the fractionation of U and Th in fluids in equilibrium with residual allanite. Allanite is essentially a rare earth and actinite containing clinozoisite or epidote. Therefore, the data on zoisite in Table 2 may be used as a proxy for allanite. Very clearly, U and Th concentrations in zoisite are about two orders of magnitude higher than in clinopyroxene or garnet. This means that the fluid/melt partition coefficients will be reduced by two orders of magnitude. Therefore, a fluid in equilibrium with allanite may very well have strongly fractionated U/Th ratios; however, the bulk concentrations of U and Th in the fluid will be so low that they cannot significantly affect the U/Th ratio of partial melts.

Conclusions

We demonstrate that: (1) U solubility in aqueous fluid strongly increases with oxygen fugacity and fluid salinity, whereas Th solubility does not (or only weakly) depend on these variables, (2) pressure increases both U and Th solubility in fluids, (3) the addition of a oxidized fluid phase with moderate fluid salinity can explain the higher U/Th ratio of the majority of arc magmas and (4) fluids in equilibrium with allanite will likely be so strongly depleted in U and Th that they cannot affect the U/Th ratio of arc magmas.

Acknowledgments The authors are grateful to Marco Scambelluri and Thomas Pettke for providing data on U/Th ratios in natural fluid inclusions. We owe thanks to Stefan Übelhack and Heinz Fischer, from the BGI machine shop, for their quick and precise work. The authors owe thanks to Professor James Brenan and three anonymous reviewers for their useful suggestions on an earlier version of this paper.

References

Aranovich LY, Newton RC (1996) H_2O activity in concentrated NaCl solutions at high pressures and temperatures measured by the brucite-periclase equilibrium. Contrib Mineral Petrol 125:200–212

Audetat A, Bali E (2010) A new technique to seal volatile-rich samples into platinum capsules. Eur J Miner 22:23–27

Audétat A, Keppler H (2005) Solubility of rutile in subduction zone fluids, as determined by experiments in the hydrothermal diamond anvil cell. Earth Planet Sci Lett 232:393–402

Bailey EH, Ragnasdottir KV (1994) Uranium and thorium solubilities in subduction zone fluids. Earth Planet Sci Lett 124:119–129

Benjamin ER, Plank T, Wade JA, Kelley KA, Hauri EH, Alvarado GE (2007) High water contents in basaltic magmas from Irazu Volcano, Costa Rica. J Volcanol Geotherm Res 168:68–92

Bertagnini A, Metrich N, Landi P, Rosi M (2003) Stromboli volcano (Aeolian Archipelago, Italy): an open window on the deep feeding system of a steady state basaltic volcano. J Geophys Res B108:2336–2351

Brenan JM, Shaw HF, Ryerson FJ, Phynney DL (1995) Mineral-aqueous fluid partitioning of trace elements at 900°C and 2 GPa: constraints on the trace element chemistry of mantle and deep crustal fluids. Geochim Cosmochim Acta 59:3331–3350

Campbell AJ, Danielson L, Righter K, Wang Y, Davidson G (2006) Oxygen fugacity at high pressure: equations of state of metal-oxide pairs. Lunar Planet Sci XXXVII Abstract #1977

Cervantes P, Wallace PJ (2003) Role of H_2O in subduction zone magmatism: new insights from melt inclusions in high-Mg basalts from central Mexico. Geology 31:235–238

Corsaro RA, Metrich N, Allard P, Andronico D, Miraglia L, Fourmentraux C (2009) The 1974 flank eruption of Mount Etna: an archetype for deep dyke-fed eruptions at basaltic volcanoes and a milestone in Etna′s recent history. J Geophys Res 114:B07204. doi: 10.1029/2008JB006013

Dorendorf F, Weichert U, Wörner G (2000) Hydrated sub-arc mantle: a source for the Kluchevskoy volcano, Kamchatka, Russia. Earth Planet Sci Lett 175:69–86

Duc-Tin Q, Audetat A, Keppler H (2007) Solubility of tin in (Cl, F)-bearing aqueous fluids at 700°C, 140 MPa: a LA-ICP-MS study on synthetic fluid inclusions. Geochim Cosmochim Acta 71:323–335

Eugster HP (1986) Minerals in hot water. Am Miner 71:655–673

Ewart A, Hawkesworth CJ (1987) The Pleistocene-Recent Tonga-Kermadec arc lavas: interpretation of new isotopic and rare earth data in terms of depleted mantle source model. J Petrol 28:495–530

Frost BR (1991) Introduction to oxygen fugacity and its petrologic importance. In: Lindsley DH (ed) Oxide minerals: petrologic and magnetic significance. Reviews in mineralogy, pp 1–9

Grove TL, Parman SW, Bowring SA, Price RC, Baker MB (2002) The role of an H2O-rich fluid component in the generation of primitive basaltic andesites and andesites from the Mt. Shasta region. N California. Contrib Miner Petrol 142:375–396

Gurenko AA, Belousov AB, Trumbull RB, Sobolev AV (2005) Explosive basaltic volcanism of the Chikurdachki Volcano (Kurile arc, Russia): insights on pre-eruptive magmatic conditions and volatile budget revealed from phenochryst hosted melt inclusions and groundmass glasses. J Volcanol Geotherm Res 147:203–232

Hakesworth C, Tuirner S, Peate D, McDermott F, van Calsteren P (1997) Elemental U and Th variations in island arc rocks: implications for U-series isotopes. Chem Geol 139:207–221

Hart SR, Blusztajn J, Dick HJB, Meyer PS, Muehlenbachs K (1999) The fingerprint of seawater circulation in a 500-meter section of ocean crust gabbros. Geochim Cosmochim Acta 63:4059–4080

Hermann J (2002) Allanite: thorium and light rare earth element carrier in subducted crust. Chem Geol 192:289–306

Hermann J, Rubatto D (2009) Accessory phase control on the trace element signature of sediment melts in subduction zones. Chem Geol 265:512–526

Hickey-Vargas R, Sun M, Lopez-Escobar L, Moreno-Roa H, Reagan MK, Morris JD, Ryan JG (2002) Multiple subduction components in the mantle wedge: evidence from eruptive centers in the Central Southern volcanic zone, Chile. Geology 30:199–202

Hill E, Wood BJ, Blundy JD (2000) The effect of Ca-Tschermaks component on trace element partitioning between clinopyroxene and silicate melt. Lithos 53:203–215

Ishimaru SA, Ishida Y, Shirashaka M, Okrugin VM (2007) Melting and multistage metasomatism in the mantle wedge beneath frontal arc inferred from highly depleted peridotite xenoliths from Avacha volcano. Southern Kamchatka. J Petrol 48:395–433

Jochum KP, Verma SP (1986) Extreme enrichment of Sb, TI and other trace elements in altered MORB. Chem Geol 130:289–299

Kamenetsky VS, Crawford AJ, Eggins S, Mühe R (1997) Phenochryst and melt inclusion chemistry of near-axis seamounts, Valu Fa Ridge, Lau Basin: insight into mantle wedge melting and the addition of subduction components. Earth Planet Sci Lett 151:205–223

Kent AJ, Peate DW, Newman S, Stolper EM, Pearce JA (2002) Chlorine in submarine glasses from the Lau Basin: seawater contamination and constraints on the composition of slab derived fluids. Earth Planet Sci Lett 202:361–377

Keppler H, Wyllie P (1990) Role of fluids in transport and fractionation of uranium and thorium in magmatic processes. Nature 348:531–533

Keppler H, Wyllie P (1991) Partitioning of Cu, Sn, Mo, W, U and Th between melt and aqueous fluid in systems haplogranite-H_2O-HCl and haplogranite-H_2O-HF. Contrib Miner Petrol 109:139–150

Kessel R, Schmidt M, Ulmer P, Pettke T (2005) Trace element signature of subduction -zone fluids, melts and supercritical liquids at 120–180 km depth. Nature 437:724–727

Kinzler RJ, Grove TL (1992) Primary magmas of mid-ocean ridge basalts 1. Experiments and methods. J Geophys Res 97:6885–6906

Klimm K, Blundy JD, Green TH (2008) Trace element partitioning and accessory phase saturation during H_2O-saturated melting of basalt with implications for subduction zone chemical fluxes. J Petrol 49:523–553

Langmuir D (1976) Uranium solution mineral equilibria at low temperatures with applications to sedimentary ore deposits. Geohemica et Cosmochemica Acta 42:547–569

Le Voyer M, Rose-Koga EF, Laubier M, Schiano P (2008) Petrogenesis of Arc lavas from the Rucu Pichincha and Pan de Azucar volcanoes (Ecuadorian arc): major, trace element, and boron isotope evidences from olivine-hosted melt inclusions. Geochem Geophys Geosyst 9/12, p 27. doi: 10.1029/2008GC002173

Lee C-TA, Leeman WP, Canil D, Li Z-X (2005) Similar V, Sc Systematics in MORB and Arc basalts: implications for the oxygen fugacities of their mantle source regions. J Petrol 46:2313–2336

Liu W, Fei P-X (2006) Methane-rich fluid inclusions from ophiolitic dunite and post-collisional mafic-ultramafic intrusion: the mantle dynamics underneath the Palaeo-Asian Ocean through to the post-collisional period. Earth Planet Sci Lett 242:286–301

Lundström CC, Shaw HF, Ryerson FJ, Williams Q, Gill J (1998) Crystal chemical control of clinopyroxene-melt partitioning in the Di-Ab-An system: implications for elemental fractionations in the depleted mantle. Geochim Cosmochim Acta 62:2849–2862

Manning CE (2004) The chemistry of subduction-zone fluids. Earth Planet Sci Lett 223:1–16

McDonough WF, Sun S-S (1995) Composition of the earth. Chem Geol 120:223–253

McInnes BIA, Gregoire M, Binns RA, Herzig PM, Hannington MD (2001) Hydrous metasomatism of oceanic sub-arc mantle, Lihir, Papua New Guinea: petrology and geochemistry of fluid-metasomatised mantle wedge xenoliths. Earth Planet Sci Lett 188:169–183

McKenzie D, O'Nions RK (1991) Partial melt distributions of rare earth element concentrations. J Petrol 32:1021–1091

Metrich N, Allard P, Spilliaert N, Andronico D, Burton M (2004) 2001 flank eruption of the alkali- and volatile-rich primitive basalt responsible for Mount Etna's evolution in the last three decades. Earth Planet Sci Lett 228:1–17

Newton RC, Manning CE (2008) Solubility of corundum in the system Al_2O_3-SiO_2-H_2O-NaCl at 800°C and 10 kbar. Chem Geol 249:250–261

Parkinson IJ, Arculus RJ (1999) The redox state of subduction zones: insights from arc-peridotites. Chem Geol 160:409–423

Pearce JA, Peate DW (1995) Tectonic implications of the composition of volcanic arc magmas. Annu Rev Earth Planet Sci 23:251–285

Peiffert C, Nguyen-Trung C, Cuney M (1994) Uranium in granitic magmas. Part 1: experimental determination of uranium solubility and fluid-melt partitioning coefficients in the uranium oxide-haplogranite-H_2O-$NaCO_3$ system at 770°C, 2 kbar. Geochim Cosmochim Acta 58:2495–2507

Peiffert C, Cuney M, Nguyen-Trung C (1996) Uranium in granitic magmas. Part 2: experimental determination of uranium solubility and fluid-melt partitioning coefficients in the uranium oxide-haplogranite-H_2O-NaX (X = Cl, F) system at 770°C 2 kbar. Geochim Cosmochim Acta 60:1515–1529

Plank T, Langmuir CH (1998) The geochemical composition of subducting sediment and its consequences for the crust and mantle. Chem Geol 145:325–394

Portnyagin M, Hoernle K, Plechov P, Mironov N, Khubanaya S (2007) Constraints on mantle melting and composition and nature of slab components in volcanic arcs from volatiles (H_2O, S, Cl, F) and trace elements in melt inclusions from the Kamchatka Arc. Earth Planet Sci Lett 255:53–69

Pownceby MI, O'Neill HSC (1994) Thermodynamic data from redox reactions at high temperatures. IV. Calibration of the Re-ReO_2 oxygen buffer from EMF and NiO + Ni-Pd redox sensor measurements. Contrib Miner Petrol 118:130–137

Quist AS, Marshall WL (1968) Electrical conductances of aqueous sodium chloride solutions from 0 to 800°C and pressures to 4000 bars. J Phys Chem 72:684–703

Roggensack K, Hervig RL, McKnight SB, Williams N (1997) Explosive basaltic volcanism from Cerro Negro Volcano: influence of volatiles on eruptive style. Science 277:1639–1642

Sakaguchi A (1999) Thermal maturity in the Shimanto accretionary prism, southwest Japan, with the thermal change of the subducting slab: fluid inclusion and vitrinite reflectance study. Earth Planet Sci Lett 173:61–74

Salters VJM, Longhi JE, Bizimis M (2002) Near mantle solidus trace element partitioning at pressures up to 3–4 GPa. Geochem Geophys Geosyst 3, p 23. doi: 10.1029/2001GC000148

Scambelluri M, Piccardo GB, Philippot P, Robbiano A, Negretti L (1997) High salinity fluid inclusions formed from recycled seawater in deeply subducted alpine serpentinite. Earth Planet Sci Lett 148:485–500

Scambelluri M, Botazzi P, Trommsdorrf V, Vannucci R, Hermann J, Gomez-Pugnaire MT, Lopez Sanchez-Vizcaino V (2001) Incompatible element-rich fluids released by antigorite breakdown in deeply subducted mantle. Earth Planet Sci Lett 192:457–470

Scambelluri M, Fiebig J, Malaspina N, Müntener O, Pettke T (2004a) Serpentine subduction: implications for fluid processes and trace element recycling. Int Geol Rev 46:595–613

Scambelluri M, Müntener O, Ottolini L, Pettke T, Vannucci R (2004b) The fate of B, Cl and Li in the subducted oceanic mantle and in the antigorite breakdown fluids. Earth Planet Sci Lett 222:217–234

Scambelluri M, Rampone E, Pettke T (2009) Serpentine dehydration recorded by garnet peridotites and chlorite harzburgites from Cima di Gagnone. Goldschmidt Abstract

Schmidt MW, Poli S (1998) Experimentally based water budgets for dehydrating slabs and consequences for arc magma generation. Earth Planet Sci Lett 163:361–379

Sharp ZD, Barnes JD (2004) Water soluble chlorides in massive seafloor serpentinites: a source of chloride in subduction zones. Earth Planet Sci Lett 226:243–254

Shaw AM, Hauri EH, Fischer TP, Hilton DR, Kelley KA (2008) Hydrogen isotopes in Mariana arc melt inclusions: implications for subduction dehydration and the deep-Earth water cycle. Earth Planet Sci Lett 275:138–145

Shock EL, Sassani DC, Betz H (1997) Uranium in geologic fluids: estimates of standard partial molal properties, oxidation potentials and hydrolysis constants at high temperatures and pressures. Geochim Cosmochim Acta 61:4245–4266

Song S, Su L, Niu Y, Lai Y, Zhang L (2009) CH_4 inclusions in orogenic harzburgite: evidence for reduced slab fluids and implication for redox melting in mantle wedge. Earth Planet Sci Lett 73:1737–1754

Spandler C, Mavrogenes J, Hermann J (2006) Experimental constraints on element mobility from subducted sediments using high-P synthetic fluid/melt inclusions. Chem Geol 239:228–249

Spilliaert N, Allard P, Metrich N, Sobolev AV (2006) Melt inclusion record of the conditions of ascent, degassing, and extrusion of volatile-rich alkali basalt during the powerful 2002 flank eruption of Mount Etna (Italy). J Geophys Res B111:4203–4222

Stolper E, Newman S (1994) The role of water in petrogenesis of Mariana trough magmas. Earth Planet Sci Lett 121:293–325

Turner S, Foden J (2001) U, Th, Ra disequilibra, Sr, Nd, and Pb isotope and trace element variations in Sunda arc lavas: predominance of subducted sediment component. Contrib Miner Petrol 142:43–57

Wallace PJ (2005) Volatiles in subduction zone magmas: concentrations and fluxes based on melt inclusion and volcanic gas data. J Volcanol Geotherm Res 140:217–240

Walter MJ (1998) Melting of garnet peridotite and the origin of komatiite and depleted lithosphere. J Petrol 39:29–60

Wood BJ, Blundy JD, Robinson AC (1999) The role of clinopyroxene in generating U-series disequilibrium during mantle melting. Geochim Cosmochim Acta 63:1613–1620

Zharikov VA, Ivanov IP, Omelyanko BI, Redkin AF, Yudintsev SV (1987) Experimental study of the solubility of uraninite in granitic melts and fluid solutions at high pressures and temperatures. Int Geol Rev 29:997–1004